17th Australasian Fluid Mechanics Conference
Auckland, New Zealand
5-9 December 2010

Numerical Simulation of a Natural Ventilation Flow with a Line Heat Source Using Various Advection Schemes

T Hattori†, S W Armfield† and M P Kirkpatrick†

†School of Aerospace, Mechanical and Mechatronic Engineering
The University of Sydney, Sydney, NSW 2006, Australia

Abstract

Two-dimensional simulations of a natural ventilation flow with a line heat source were conducted to compare different advection schemes and to investigate the turbulent structure of this flow. The flow was simulated at a Prandtl number of 7, and a Reynolds number of 5×10^5 based on the height of enclosure and the source buoyancy. A preliminary three-dimensional simulation was also conducted to study the effect of any three-dimensionality in the flow.

Introduction

Air-conditioning has been a serious issue in recent energy-saving and environmental themes. Accordingly, natural ventilation with reduced energy demand and reduced CO_2 emissions has started to attract much attention as a potential alternative to conventional ventilation. For the optimisation of performance, the detailed fluid mechanics of natural ventilation flows, including turbulence, needs to be understood. This may be efficiently and economically accomplished using numerical simulation techniques.

Numerical simulation techniques have been widely used in the study of ventilation and buoyancy-driven flows. In most of the past studies, the Reynolds-Averaged Navier-Stokes (RANS) methods were adopted. A natural ventilation flow with a line heat source was also studied by Cook and Lomas [3] using the standard $k-\varepsilon$ model and the Re-Normalisation Group (RNG) $k-\varepsilon$ model. Their numerical results were shown to be comparable to the experimental and theoretical work of Linden et al. [9]. Some discrepancies were, however, considered to be due to an incorrect modelling of the entrainment in a turbulent plume. As mentioned in [4, 8, 9], this mechanism is the fundamental factor affecting the overall flow mechanics, hence a correct modelling of this mechanism is crucial in simulating such flows. Turbulent plume entrainment is primarily carried out by large eddies across the plume boundary [10]. In conventional RANS methods all the unsteadiness is averaged out, with even the largest scale motions removed. Such methods are therefore considered to be undesirable in the current study.

The most accurate numerical method is direct numerical simulation (DNS) in which all the scales of turbulent motion are resolved, requiring the grid size to be smaller than the Kolmogorov length scale. In the current study, two-dimensional simulations were conducted with the mesh resolutions of 603×425 and 453×325, with smallest, non-dimensional grid sizes of 0.001 and 0.0015, respectively. For a flow simulation with the Reynolds number of 5×10^5 and the height of the enclosure as the length scale, the non-dimensional Kolmogorov length scale for two-dimensional turbulence ($\propto Re^{-\frac{1}{2}}$) is computed to be $\propto 0.00141$. Thus, these mesh resolutions may be considered to be fine enough to sufficiently resolve all the scales of motions. Grid dependency results will be shown for these mesh resolutions in the following section. DNS is, however, very expensive and impractical in many applications involving three-dimensional high Reynolds-number flows. The non-dimensional Kolmogorov length scale computed for a simulation of three-dimensional turbulence ($\propto Re^{-\frac{3}{4}}$) with the same Reynolds number and the same length scale is $\propto 5.318 \times 10^{-5}$. Therefore, a three-dimensional DNS is not feasible in the current study using currently available facilities. As a preliminary study, a three-dimensional simulation was conducted with an under resolved mesh of $373 \times 267 \times 20$ to investigate the effect of any three-dimensionality of the flow.

In this study, two-dimensional simulations of a natural ventilation flow with a line heat source were conducted to compare the effects of different advection schemes and to investigate the turbulent structure of this flow. Further, a preliminary three-dimensional simulation was conducted to study the effect of any three-dimensionality of the flow. Numerical results are compared to the experimental and theoretical work of [9].

Numerical method

The simulations were designed to approximate the small scale experiments of a natural ventilation flow with a line source of buoyancy, previously conducted by Linden et al. [9]. Dimensions are given in figure 1. As shown, the geometry is symmetrical about the source. The centre of the source is located at $(x,y) = (1.0, 0.0)$ (non-dimensional). The flow is simulated at a Prandtl number (Pr) of 7 and Reynolds number (Re) of 5×10^5, based on the domain height ($H = 0.25m$) and source buoyancy, where $Re = \sqrt{g\beta\Delta TH} \times H/\nu$ with ν the kinematic viscosity. $U = \sqrt{g\beta\Delta TH}$ is the characteristic velocity scale, where β is thermal expansion coefficient, g the gravitational acceleration and ΔT the characteristic temperature scale defined as $\Delta T = T_y H$. T_y is the temperature gradient at the source and is related to the source heat flux per unit length, W_L, by $W_L = kA_L T_y$, where k is thermal conductivity and A_L the source area per unit length. Froude number, Fr, is defined as $Fr = U/\sqrt{g\beta\Delta TH}$, hence Fr is unity, i.e. the flow is independent of Fr. The governing equations are the non-dimensional, incompressible Navier-Stokes equations with the Boussinesq assumption. Variables are stored on a non-staggered, Cartesian grid, and the equations are solved using the finite volume method. A non-uniform mesh is used to provide the greatest resolution near the source and openings. Different advection schemes are employed in the energy equation for the sake of comparison, while second order central differencing is used for the diffusion term and in the momentum equations. Advection schemes tested are second order central differencing (**CD2**), fourth order central differencing (**CD4**), CD2 with the ULTRA (Universal Limiter for Tight Resolution and Accuracy) flux limiter [7] (**ULTRA2**) and CD4 with the ULTRA flux limiter (**ULTRA4**). The Adams-Bashforth and the Crank-Nicolson schemes are used for the temporal discretisation of the advection and diffusion terms, respectively. The fractional step method [2] with the velocity interpolation scheme of [1] is used for the velocity-pressure coupling. A Jacobi solver is used for the momentum and energy equations and the Bi-Conjugate Gradient Stabilised method (BiCGSTAB) with a Jacobi precon-

ditioner for the Poisson pressure correction equation. The required convergence criteria are that *residual* $< 1 \times 10^{-8}$ for the Jacobi solver and *residual* $< 3 \times 10^{-9}$ for the BiCGSTAB. The

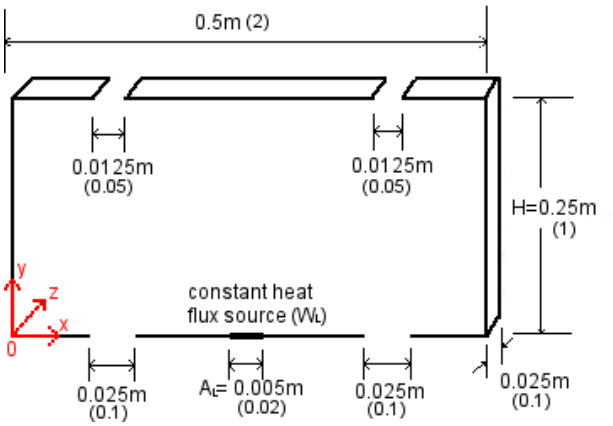

Figure 1: Geometry of the enclosure under consideration, with the corresponding non-dimensional values given inside brackets. The coordinate system and the location of the origin are as shown.

code is written in the FORTRAN90 language. The boundary conditions are as follows.

- On closed boundaries, the no-slip condition is applied for velocity and the Neumann condition with zero derivative for pressure correction. Pressure on the external node is obtained by a second order extrapolation.
- On open boundaries, the tangential velocity and pressure correction are set to zero. On the top openings, the Neumann condition with zero derivative is applied for the normal velocity component, and pressure is set to zero on the external node. On the bottom openings, the normal velocity component is calculated such that the rate of inflow through the bottom openings is equal to the rate of outflow through the top openings, with pressure on the external node obtained by a second order extrapolation. To determine the effect of the different advection schemes on the turbulent structure, simulations are also conducted with the normal velocity component on the bottom openings fixed at 1.5×10^{-3}, since this allows a more direct comparison.
- Boundary walls are all adiabatic except for the source and the inlets. At the constant heat flux source, $\partial T/\partial y$ is set to -1.0, and the inflow temperature is set to $T = 0$.
- For the three-dimensional simulation, a periodic boundary condition is applied in the z direction.

A non-dimensional time step of 0.01 is used for the mesh resolutions of 453×325 and $373 \times 267 \times 20$, and 0.0075 for 603×425. This keeps the Courant number in the range of 0.015-0.03 for the fully developed flows.

Two-dimensional simulation results

Comparison of advection schemes

The aforementioned four different advection schemes (**CD2**, **CD4**, **ULTRA2** and **ULTRA4**) were employed in the energy equation to compare their effects on mean temperature field and on the turbulent structure. *Mean temperature* plotted in the following figures refers to temporal mean, spatially averaged across the domain width. The temporal mean was obtained using 3×10^6 time steps after full development of the flow. Firstly, the results for mean temperature field obtained with the different mesh resolutions, using the different schemes, are presented to show grid dependency of the results and to examine the accuracy of the results with the different schemes by benchmarking against the experimental and theoretical work of [9]. This is followed by a comparison of the effect of the different schemes on the turbulent structure, for which results were obtained with a fixed inlet velocity boundary condition.

Linden et al. [9] developed theoretical models which relate steady-state interface height (h) and reduced gravity in the upper warm layer (g') to geometry, the source buoyancy per unit length (B_L) and the entrainment constant (α) as follows:

$$\frac{A_L^*}{H} = 2\alpha \left(\frac{\xi^3}{1-\xi} \right)^{\frac{1}{2}}, \tag{1}$$

$$\frac{g'}{G'_H} = \frac{1}{\xi}. \tag{2}$$

$\xi = h/H$ is the non-dimensional interface height. A_L^* is the effective opening area per unit length calculated as $A_L^* = a_t a_b / \left\{ \frac{1}{2} \left(a_t^2 + a_b^2 \right) \right\}^{\frac{1}{2}}$, where a_t and a_b are the areas of top and bottom openings per unit length, respectively. In equation (2), g' is non-dimensionalised by $G'_H = B_L^{\frac{2}{3}} / (2\alpha)^{\frac{2}{3}} H$, the reduced gravity inside a plume at the ceiling height. B_L is calculated as $B_L = g\beta W_L / \rho C_p$, where ρ is fluid density and C_p the specific heat at constant pressure. α, the entrainment constant, is assumed to be 0.1 [3]. For the current geometry where $A_L^*/H = 0.1265$, Linden et al. [9] obtained $\xi \simeq 0.52$ (experimental) and $\simeq 0.56$ (theoretical), and $g'/G'_H \simeq 2.4$ (experimental) and $\simeq 1.8$ (theoretical) (refer to figure 13 of [9]). In figure 2, the mean temperature obtained here is plotted against the domain height for the different advection schemes and for the different mesh resolutions (453×325 and 603×425). Firstly, comparing the variation in the results with the different advection schemes, it is apparent that refining the grid is leading to a reduced variation as expected. In the derivation of equations (1) and (2), a well-mixed upper layer of uniform buoyancy was assumed [9]. In figure 2, there is a sudden, large increase in the mean temperature in the range $0.2 \lesssim \textit{height} \lesssim 0.4$, followed by a smaller increase in the range $0.4 \lesssim \textit{height} \lesssim 0.6$ and almost constant temperature for $\textit{height} \gtrsim 0.6$ for all the results. Thus, based on the above assumption [9], the interface height may be assumed in the range $0.4 \lesssim \textit{height} \lesssim 0.6$. Regarding the mean temperature above the interface, there is a larger variation in the results with the different schemes when the coarser mesh resolution of 453×325 was employed than in the case with the finer mesh of 603×425, as previously mentioned. Hence, for the sake of comparison of the different schemes, the values of g'/G'_H were obtained based on the results for the mesh resolution of 453×325. The mean temperature above the interface is approximately 2.0×10^{-5} for **CD2** and **ULTRA4**. g' is calculated as $g' = g(\rho_0^* - \rho^*)/\rho_0^* = g\beta(T^* - T_0^*) = g\beta\Delta T \times T$, where superscript * and subscript $_0$ denote dimensional and reference values, respectively, and T is non-dimensional temperature. Rewriting W_L and B_L using the definitions for Re, Pr ($= \nu\rho C_p/k$), U and ΔT, g'/G'_H is expressed as:

$$\frac{g'}{G'_H} = \left(\frac{2\alpha \times Re \times Pr \times H}{A_L} \right)^{\frac{2}{3}} \times T. \tag{3}$$

This gives $g'/G'_H \simeq 2.1$ for $T = 2.0 \times 10^{-5}$. For **CD4** and **ULTRA2**, the mean temperature above the interface is approxi-

mately 2.3×10^{-5} and 2.5×10^{-5} with $g'/G'_H \simeq 2.5$ and $\simeq 2.7$, respectively. Thus, the results for all the tested schemes show a reasonable agreement with the experimental values. However, **CD2** and **ULTRA4** may be considered to be the most accurate schemes since their g'/G'_H lie between the experimental and theoretical values, and these schemes show the smallest grid dependency. Furthermore, a non-physical, negative temperature field was found in instantaneous temperature fields for **CD2** and **CD4**. Therefore, **ULTRA4** may be considered to be the best advection scheme amongst the four schemes tested.

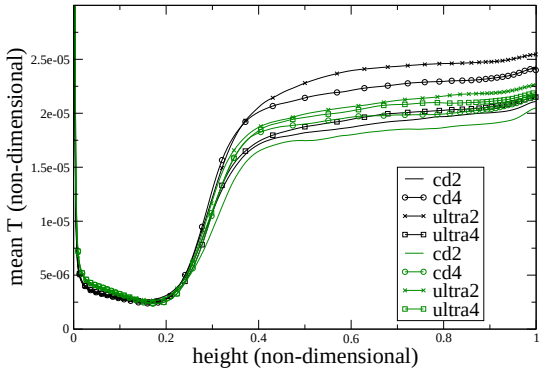

Figure 2: Mean temperature along the domain height for the different advection schemes with the mesh resolutions of 453×325 (black) and 603×425 (green)

To determine the effect of the different schemes on the turbulent structure, results were obtained with a fixed inlet velocity of 1.5×10^{-3}, and spectra were examined. The temporal spectra of the vertical velocity component at a point above the source, $(x,y)=(1.0,0.15)$, shown in figure 3 were obtained over 4 million time steps after full development of the flow, for a mesh resolution of 453×325 with a time step of 0.01. The spectra are plotted against non-dimensional frequency, $St=f^*_{temporal}\times\tau$, where $f^*_{temporal}$ is dimensional frequency and $\tau=H/U$ the characteristic time scale. The non-dimensional Nyquist frequency, St_{max}, is 50. Spectral amplitudes are almost the same for the different schemes in the lower frequency range ($St\lesssim0.05$). However, smaller spectral amplitudes were found for **ULTRA2** and **ULTRA4** than **CD2** and **CD4** at higher frequencies. This is considered to be due to the diffusive nature of flux-limited schemes. All the spectra show the $-5/3$ and -3 power laws, as discussed in the following section, in the ranges $0.003\lesssim St\lesssim0.02$ and $0.02\lesssim St\lesssim0.1$, respectively.

Turbulence

To further investigate the turbulent structure of the flow, using two-dimensional simulations, both spatial and temporal spectra have been obtained on the finer mesh resolution of 603×425. The following results were obtained with the usual boundary condition where the inlet velocity is calculated from the rate of outflow. Figure 4 shows the spatial spectrum of the instantaneous vertical velocity component in the vicinity of the plume source obtained using the **CD2** advection scheme. In this region uniform grid sizes of $\Delta x=\Delta y=0.001$ were adopted. The spatial spectrum is plotted against non-dimensional frequency defined as $f=f^*_{spatial}\times H$, where $f^*_{spatial}$ is dimensional frequency. The non-dimensional Nyquist frequency, f_{max}, is 500. Figure 5 shows the temporal spectra of the vertical velocity component at different heights along the plume axis, obtained over 4.5 million time steps after full development of the flow, with **ULTRA4** and a time step of 0.0075. The spectra are plotted against non-dimensional frequency, St. The non-dimensional Nyquist frequency, St_{max}, is 67. Both results show that most energy is contained in large scale, low frequency motions, with negligible energy in grid scale, high frequency ones.

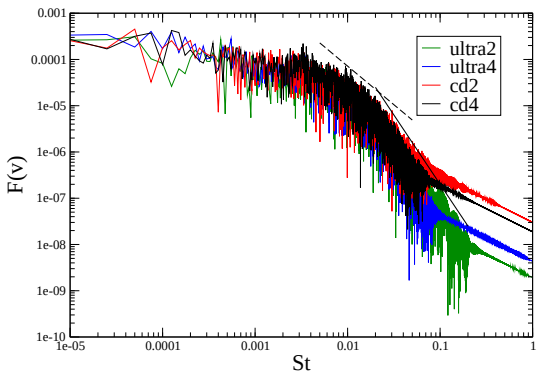

Figure 3: Temporal spectra of the vertical velocity component at a point above the source, $(x,y)=(1.0,0.15)$, for different advection schemes with the inlet velocity fixed at 1.5×10^{-3}, where the solid line and the dashed line show the slope of -3 and $-5/3$, respectively

As shown in figure 5, the energy decay follows the $-5/3$ power law in the range $0.004\lesssim St\lesssim0.03$, while the -3 power law is followed in the range $0.03\lesssim St\lesssim0.1$ as expected for two-dimensional turbulence [5, 6]. Spectral amplitudes were found to be reduced at $y=0.95$, inside the upper warm layer, from those at $y=0.15$ and $y=0.5$. This phenomenon may be considered to be due to enhanced dissipation by buoyancy effects.

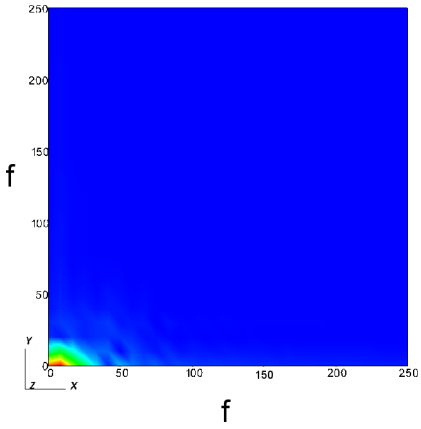

Figure 4: Spatial spectrum of the instantaneous vertical velocity component in the vicinity of the plume source, $\{0.94\le x\le1.06,\ 0\le y\le0.1\}$ (The region coloured in red corresponds to the value of 3.159, yellow 2.369, green 1.580, light blue 0.790 and blue 0.0004021.)

Three-dimensional effects

In this section, the results of a preliminary three-dimensional investigation are presented and discussed. A simulation was con-

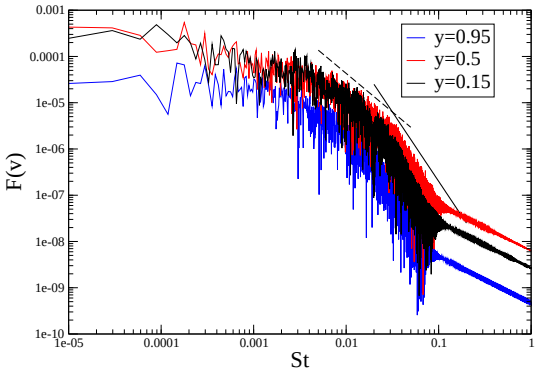

Figure 5: Temporal spectra of the vertical velocity component at different heights along the plume axis ($x = 1.0$) where the solid line and the dashed line show the slope of -3 and $-5/3$, respectively

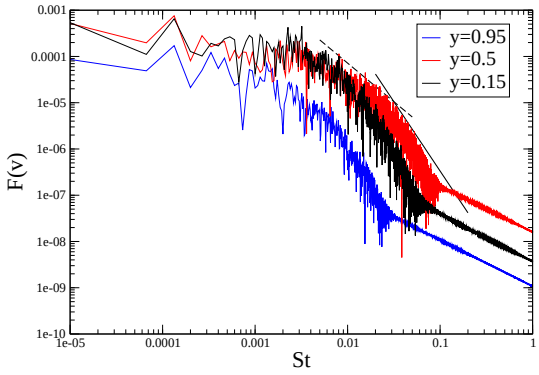

Figure 6: Three-dimensional simulation results for temporal spectra of the vertical velocity component at different heights along the line, $(x,z) = (1.0, 0.05)$ where the solid line and the dashed line show the slope of -3 and $-5/3$, respectively

ducted using a mesh resolution of $373 \times 267 \times 20$ with a time step of 0.01 and **CD2** in the energy equation. A uniform mesh was used in the z direction with $\Delta z = 0.005$. The magnitude of the maximum velocity in the spanwise (z) direction was found to be very small, typically in the order of $1 \times 10^{-9} - 1 \times 10^{-8}$. In figure 6, the temporal spectra of the vertical velocity component at different heights along the line, $(x,z) = (1.0, 0.05)$, are plotted against St for the preliminary three-dimensional simulation. St_{max} here is 50. The spectra were obtained using 1.5×10^6 time steps. Compared with figure 5, the spectral amplitudes are slightly higher at $y = 0.15$ and $y = 0.5$, while they are slightly smaller at $y = 0.95$. Such discrepancies are considered to be due to the coarse (under resolved) mesh resolution and fewer time steps used in this case. However, the basic structures of the 3D spectra are the same as the 2D spectra plotted in figure 5, showing the $-5/3$ and -3 power laws in the frequency ranges of $0.006 \lesssim St \lesssim 0.03$ and $0.03 \lesssim St \lesssim 0.1$, respectively, and with the largest amplitudes at $y = 0.5$. From the above results, for the current Reynolds and Prandtl numbers, it is reasonable to conclude that the three-dimensional effects are negligible, and hence the two-dimensional simulation results presented in this paper are reliable.

Conclusion

In this study, the effects of the different advection schemes were compared, and the turbulent structure of the flow was investigated, using two-dimensional simulations. Also, a preliminary three-dimensional investigation was conducted to study the effect of the three-dimensionality. The results for the mean temperature field with **CD2** and **ULTRA4** show the best agreement with the work of Linden et al. [9], with **ULTRA4** having no non-physical under- and over-shoots in the temperature field, in contrast to **CD2** and **CD4**. Reduced spectral amplitudes were found for the flux-limited schemes of **ULTRA2** and **ULTRA4**, as expected. Temporal and spatial spectra show that most energy is contained in low frequency motions. From a preliminary three-dimensional simulation, the velocity in the z direction was found to be very small, and the spectral plot shows similar features to those obtained from a two-dimensional simulation. Both of these results show the -3 power, as expected for two-dimensional turbulence [5, 6]. Therefore, it is concluded that the three-dimensionality has negligible effects, and hence the two-dimensional simulation results presented in this paper are reliable.

*

References

[1] Armfield, S. W., Ellipticity, accuracy, and convergence of the discrete navier-stokes equations, *J. Comput. Phys.*, **114**, 1994, 176–84.

[2] Armfield, S. W. and Street, R., An analysis and comparison of the time accuracy of fractional-step methods for the navier-stokes equations on staggered grids, *Int. J. Numer. Methods Fluids*, **38**, 2002, 255–82.

[3] Cook, M. and Lomas, K., Buoyancy-driven displacement ventilation flows: Evaluation of two eddy viscosity turbulence models for prediction, *Building Service Engineering*, **19**, 1998, 15–21.

[4] Hunt, G. R. and Linden, P. F., Steady-state flows in an enclosure ventilated by buoyancy forces assisted by wind, *J. Fluid Mech.*, **426**, 2001, 355–86.

[5] Kraichnan, R. H., Inertial ranges in two-dimensional turbulence, *Phys. Fluids*, **10**, 1967, 1417–23.

[6] Kraichnan, R. H. and Montgomery, D., Two-dimensional turbulence, *Rep. Prog. Phys.*, **43**, 1980, 547–619.

[7] Leonard, B. P. and Mokhtari, S., Beyond first-order upwinding: The ultra-sharp alternative for non-oscillatory steady-state simulation of convection, *Int. J. Numer. Methods Eng.*, **30**, 1990, 729–66.

[8] Linden, P. F., The fluid mechanics of natural ventilation, *Annu. Rev. Fluid Mech.*, **31**, 1999, 201–38.

[9] Linden, P. F., Laneserff, G. F. and Smeed, D. A., Emptying filling boxes - the fluid-mechanics of natural ventilation, *J. Fluid Mech.*, **212**, 1990, 309–35.

[10] Turner, J. S., Buoyant plumes and thermals, *Annu. Rev. Fluid Mech.*, **1**, 1969, 29–&.